*metals*

MDPI

*Article*

# Estimation Method of Relative Slip in Fretting Fatigue Contact by Digital Image Correlation

**Yue Su [1,2], Shao-Shi Rui [1,3], Qi-Nan Han [4,5], Zhi-Hao Shang [1], Li-Sha Niu [1], Hao Li [6], Hiroshi Ishikawa [6] and Hui-Ji Shi [1,*]**

1 AML, School of Aerospace Engineering, Tsinghua University, Beijing 100084, China; suy@nwpu.edu.cn (Y.S.); ruishaoshi@imech.ac.cn (S.-S.R.); troygol@126.com (Z.-H.S.); niulsh@tsinghua.edu.cn (L.-S.N.)
2 School of Power and Energy, Northwestern Polytechnical University, Xi'an 710129, China
3 LNM, Institute of Mechanics, Chinese Academy of Sciences, Beijing 100190, China
4 College of Energy and Power Engineering, Nanjing University of Aeronautics and Astronautics, Nanjing 210016, China; hanqn@nuaa.edu.cn
5 Aero-Engine Thermal Environment and Structure Key Laboratory of Ministry of Industry and Information Technology, Nanjing 210016, China
6 Strength Research Department, Research & Innovation Center, Mitsubishi Heavy Industries, Ltd., Takasago 676-8686, Japan; hao.li.j8@mhi.com (H.L.); hiroshi.ishikawa.j5@mhi.com (H.I.)
* Correspondence: shihj@mail.tsinghua.edu.cn; Tel.: +86-(10)-6277-2731

**Abstract:** An experimental method that can quantify relative slip was developed using digital image correlation (DIC) in order to evaluate the sliding portion. The bridge-type test setup was designed to establish the fretting contact condition. The relative displacements between the contact surfaces were determined by DIC methods. Based on the evolution and distribution of relative slip, the transitions from gross slip to partial slip on the contact surface were found throughout all tests. This result indicated that the fretting scar was closely correlated to relative slip. The variation of relative slip corresponding to the stick-slip state was consistent with the tangential force coefficient. Besides, the load amplitude was an important factor for fretting fatigue damage, which can affect the stick-slip state.

**Keywords:** fretting fatigue; digital image correlation; relative slip; tangential contact stiffness



**Citation:** Su, Y.; Rui, S.-S.; Han, Q.-N.; Shang, Z.-H.; Niu, L.-S.; Li, H.; Ishikawa, H.; Shi, H.-J. Estimation Method of Relative Slip in Fretting Fatigue Contact by Digital Image Correlation. *Metals* **2022**, *12*, 1124. https://doi.org/10.3390/met12071124

Academic Editor: Tilmann Beck

Received: 24 May 2022
Accepted: 28 June 2022
Published: 30 June 2022



## 1. Introduction

Fretting fatigue occurs between two solid surfaces in contact with a small relative displacement (usually less than 100 μm) due to the oscillating or cyclic bulk force [1–3]. This condition leads to severe surface degradation and crack initiation, which will reduce the life of components, such as railway axles [4,5], rivet holes [6,7], bolted joints [8], and ropes [9]. Especially, the fretting damage at the blade root attachments in the turbine and compressor has been widely reported, which is caused by centrifugal and aerodynamic force [10–13]. Thus, more and more researchers' attentions are focused on the fretting fatigue at the turbine blade-disk attachments.

Many studies have shown that the fretting behavior largely depends on the slip amplitude between contact surfaces [14–16]. If the remotely applied relative displacement amplitude is large enough, all points on the contact surface will undergo sliding, which is known as the gross slip condition. Conversely, some parts of the contact surfaces remain stuck when the remotely applied relative displacement amplitude is low. Therefore, the contact surface includes the slip zone and stick zone, and this is referred to as the partial slip. At the same time, the damage caused by fretting is closely related to the slip condition [17–19]. The fretting wear mainly occurs in gross slip, while the fretting fatigue is more significant in partial slip. Vingsbo [20] pointed out that the number of load cycles first decreases and then increases with increasing slip amplitude under fretting experiments. Additionally, the minimum fretting life occurs at the transition from partial

slip to gross slip. The effect of slip on fretting fatigue life was also observed by Jin and Mall [21]. In addition, experimental studies have proved that the fretting crack behavior is usually closely related to the slip or stick state of contact surfaces. For example, the fracture morphology [22,23] and in situ observation [24,25] have clearly shown that the fretting cracks nucleate at the stick-slip interface. Thus, the slip amplitude measurement under fretting tests is still needed in order to distinguish the stick or slip region on the contact surfaces.

The measurement methods of slip amplitude have been widely reported in the literature [26–31]. For example, Wittkowsky et al. [26] used an extensometer assembly to measure the relative displacement between the fretting and specimen. The clip gauge was installed on the sample and fretting pad to monitor the relative displacement between the contact surfaces by Pauw et al. [30]. Besides, Ding et al. [31] performed a fretting fatigue experiment and completed the slip measurement by the linear variable differential transformers (LVDT). However, the results obtained by the above methods cannot reflect the true relative displacement on both sides of the contact surface. Since the two contact feet of measuring equipment were connected to the sample and fretting pad, they were at a certain distance from the contact surfaces. The measurement result only represents the relative displacement of two points, rather than the distribution of the relative displacement along the contact surfaces. This not only is remote data but also includes the elastic deformation of surrounding material. Furthermore, the deformation of the complicated device was also included in the slip results. In short, it is challenging to accurately measure the small relative slip between the contact surfaces under fretting conditions.

Recently, aside from the conventional methods mentioned above, the relative displacement between the fretting contact surfaces has also been studied by digital image correlation (DIC). Based on the gray level of the image, the DIC method is a noncontact full-field deformation optical measurement technique [32,33] Juoksukangas et al. [34,35] performed cantilever beam bending tests to simulate the fretting contact state. The DIC technique was used to quantify the local relative displacement field at the fretting contact interface and minimize the effect of test device compliances. Crevoisier et al. [36] obtained displacement jump in bolted assembly by the DIC method. Additionally, the in situ frictional properties of a fretting surface, such as friction coefficient and secant stiffness, were identified. Besides, Kartal [29] and Pauw [30] employed the DIC method to describe the hysteresis loop during macroscale fretting fatigue tests. These results show that the tangential contact stiffness depends highly on the normal pressure and contact area. However, their works were limited to an overall slip value of the entire contact surface. The distribution and evolution of the slip along the contact surface were rarely reported. It is impossible to give the stick-slip state of the contact surface under partial slip condition. Therefore, in order to obtain the ideal displacement data, it is necessary to develop a novel measurement method based on the DIC technique with a higher pixel and accuracy.

This paper aims to grasp the distribution and evolution of the stick-slip zone between the contact surfaces under fretting conditions. The DIC technique was employed to measure the relative displacement field between the contact interfaces. Then a method that can be used to evaluate the sliding part of the contact surface under fretting fatigue was established. For this purpose, Section 2 introduces fretting fatigue experiments to simulate the fretting fatigue behavior of the blade-disk attachments in a turbine engine. Additionally, a novel optical system was built in Section 2. Section 3 presents the hysteresis loops of relative displacement and tangential force. The slip values and tangential contact stiffness during the fretting fatigue tests were determined in Section 4. Then the distribution of the stick-slip state along the contact surfaces was obtained under the fretting conditions. Besides, the effect of cyclic load amplitude on fretting properties was investigated. Finally, the conclusions are summarized in Section 5.

## 2. Materials and Experiment

For the experimental work, the bridge-type device was suitable for simulating the fretting fatigue conditions in the laboratory. A camera was used to implement DIC for the measurement of the relative displacement between the contact surfaces. In the following sections, detailed information on the experimental configuration will be given.

### *2.1. Material and Sample*

The material chosen for this paper was SUS410 stainless steel. This alloy is widely used in a turbine or compressors due to its excellent mechanical properties [37]. The typical mechanical properties are listed in Table 1, which are obtained from tensile tests based on the ASTM E08 standard [38]. All specimens and fretting pads were made from the same plate of stainless steel.

**Table 1.** Mechanical properties of SUS410 steel in this work.

| Young's Modulus (GPa) | Proportionality Limit (MPa) | 0.2% Proof Stress (MPa) | Tensile Strength (MPa) | Elongation (%) | Poisson's Ratio |
|---|---|---|---|---|---|
| 212.31 | 438.29 | 539.52 | 715.44 | 28.78 | 0.26 |

The geometries of the specimen and fretting pad are shown in Figure 1. These dimensions are prepared according to the JSME standard [39]. As can be seen from the figure, the fretting pad has two contact feet, and each of which has a 3.1 mm flat surface with rounded edges of R = 0.2 mm. This foot is in contact with the flat side of the dog-bone specimen (see Figure 2). The thicknesses of the dog-bone specimen and fretting pad are 6 mm. There are no edges in the thickness direction to ensure complete contact. Thus, the area of the contact surface is 3.1 × 6 $mm^2$. All specimens and fretting pads were machined by wire electrical discharge machining, and the contact surfaces were both ground and polished to reduce the finish surface roughness (Ra = 0.4 μm).

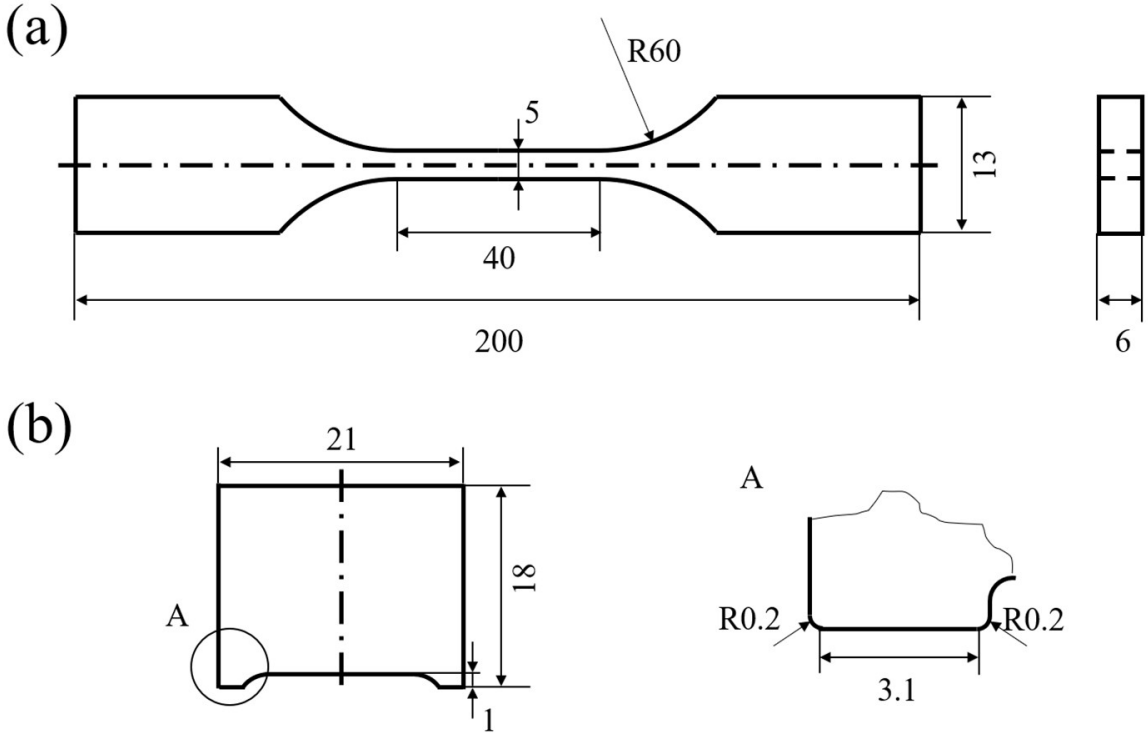


**Figure 1.** Dimensions of the (**a**) specimen and (**b**) fretting pad (all dimensions are in mm).

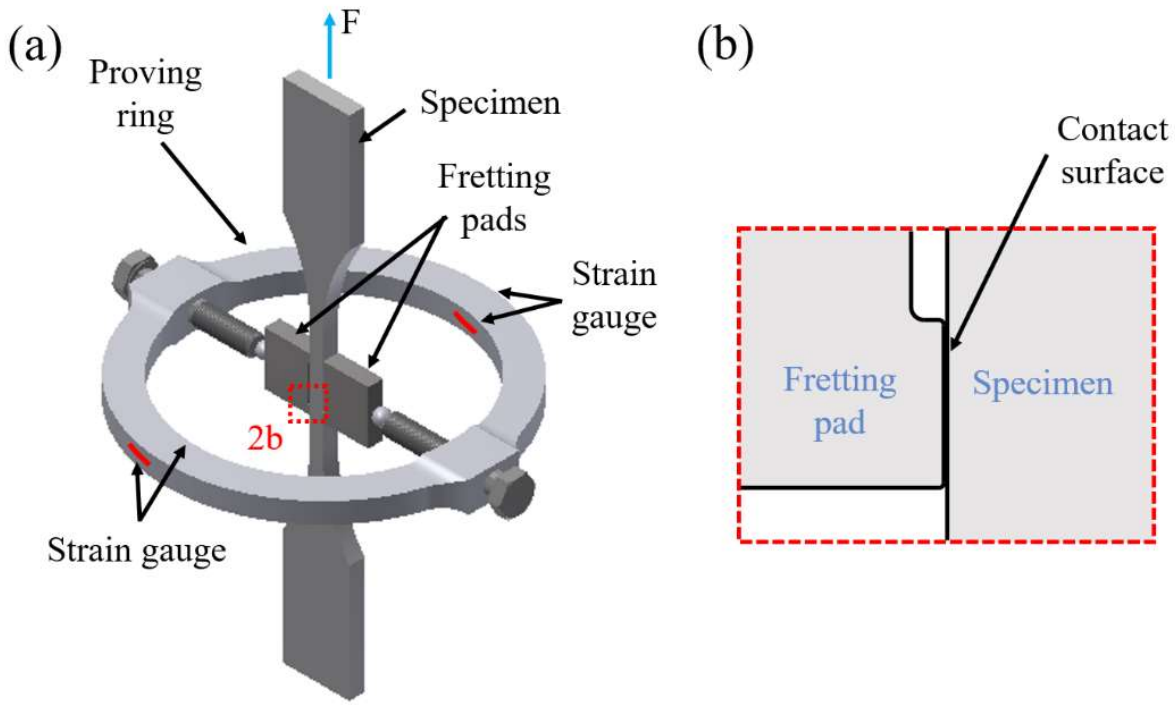


**Figure 2.** Schematic diagram of (**a**) the fretting fatigue experimental setup and (**b**) the contact surface between the fretting pad and specimen.

### *2.2. Fretting Fatigue Test*

An experimental setup was designed to simulate the fretting contact condition, which is based on the JSME standard [39]. A schematic of the bridge-type fretting fatigue test apparatus is shown in Figure 2. Two fretting pads were pressed on the side of the dog-bone specimen. The proving ring and screw were used to apply the normal contact force between the specimen and fretting pads. The dog-bone specimen was mounted on the servo-hydraulic fatigue testing machine (Instron 8801). Then, the upper end of the specimen was fixed by the chuck, and the cyclic load was applied to the specimen along the length direction by the movement of the lower gripper. Hence, a total of four flat-on-flat fretting contact surfaces (Figure 2b) were formed between the specimen and fretting pads. This is a typical contact form for the fir-tree-type blade-disk attachment in the turbine engine. Since the contact was in plane strain state, the bending of the fretting pads was ignored. As shown in Figure 2a, four strain gauges were used to monitor the normal contact force, which are attached at the proving ring. These results of strain gauges revealed that the force value was changed only slightly during the testing. A strain gauge was installed between the fretting pad contact feet, and the tangential force ($F$t) was calculated from the corresponding strain values. More detailed information about measurement methods can be found in the literature [39,40]. In this fretting fatigue test, these strain values were collected at a frequency of 1000 Hz.

In this paper, the fretting fatigue test was carried out at room temperature. These test parameters are listed in Table 2. The normal contact pressure in the horizontal direction was chosen to be 90 MPa, according to the deformation of the proving ring, during which the screw is tightened. This roughly presents the normal contact pressure in the actual designs of the blade-disk attachment. A sinusoidal cyclic load with a frequency of 20 Hz was axially applied to the specimen. The stress ratio of the applied cyclic load was set as −1. In order to investigate the effect of cyclic load amplitude ($F$a) on the fretting fatigue behavior, three different load levels (8.5, 7.3, and 6.5 kN) were used in our work. The nominal stress amplitudes corresponding to three different load amplitudes were 283.33, 243.33, and 216.67 MPa. Before the test, all contact surfaces were cleaned with acetone. Additionally, marks were made in the vertical and horizontal

directions of the specimen. Then, the specimen position was adjusted in the camera field of view in order to ensure alignment. Each test was conducted until the specimen broke or the number of cycles reached 200,000.

**Table 2.** Loading parameters of the fretting fatigue test in this work.

| Stress Ratio | Frequency | Waveform | Cyclic Load Amplitude (*Fa*) | Average Normal Pressure |
|---|---|---|---|---|
| −1 | 20 Hz | Sine wave | 8.5, 7.3, 6.5 kN | 90 MPa |

### *2.3. Digital Image Correlation (DIC)*

The DIC method was used to measure the full-field displacement at the contact region during the above fretting fatigue testing, which is a well-known established technique in experimental mechanics [41,42]. The complete test system is shown in Figure 3, which includes the fretting fatigue setup, optical device, and strain measurement equipment. It can be seen from the figure that the fretting fatigue setup was installed on the fatigue testing machine, and was axially loaded with periodical force. Two lights were used to improve image quality. The speckle pattern was spraying on the surface of the specimen and fretting pads, and the diameter of one black spot was approximately 50 μm. This change in speckle was monitored during each experiment by a camera with a resolution of 2448 × 2050 pixels (5 megapixels). Since four contact surfaces were similar, only the lower contact region (Figure 4a) was observed during the measurement. A rectangular field of interest was recorded at a rate of 1 Hz. As shown in Figure 4b, a contact surface was found in this observation view. The frequency of the fretting fatigue test was reduced from 20 to 0.05 Hz during DIC measurement. Therefore, about 20 image data points were measured in each fatigue cycle. The tangential force was measured at two frequencies (20 and 0.05 Hz). The results show that the difference in tangential force was relatively slight. Then, the displacement field can be calculated by the correlation algorithms based on the deformed image. Table 3 summarizes the postprocessing parameters. A subset of 101 × 101 pixels was used in this work, and the step was set as 15 pixels. Before the formal test, two images were continuously recorded when the fretting fatigue setup was at rest in order to determine the displacement measurement accuracy. Then, repeated measurements were carried out for the same static state. Based on the above postprocessing parameters, the measurement error of vertical displacement is less than 1 μm.

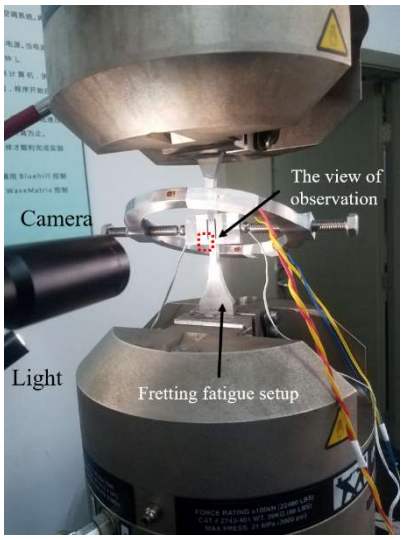


**Figure 3.** Photograph of the complete experimental setup in this study (The magnified area of the red wireframe is the field of view observed by the camera).

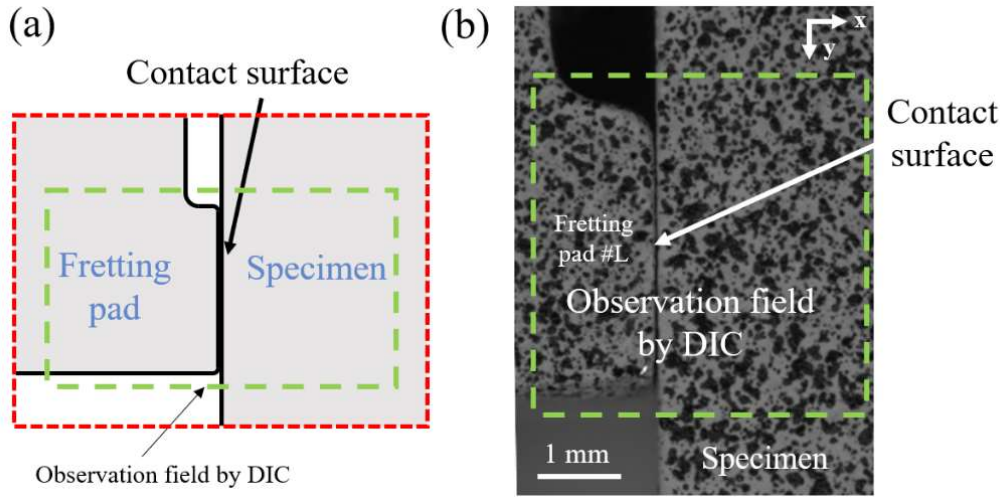


**Figure 4.** (**a**) Schematic diagram of the observation field for the DIC measurement and (**b**) observation field captured by the camera during the test.

**Table 3.** DIC measurement parameters used in this work.

| Camera Pixel | Field of View | Sampling Rate | Subset | Step |
|---|---|---|---|---|
| 5 megapixels (2448 × 2050) | 8.8 × 6.6 mm$^2$ | 20 images/cycle | 101 × 101 pixels | 15 pixels |

## 3. Experimental Results

### *3.1. Fretting Scar*

As a result of the fretting damage, fretting scars were observed on all contact surfaces of the specimen and fretting pad after the experiment. Notice that the marks on the left and right contact surfaces were similar due to the symmetry of the fretting fatigue experimental setup. Therefore, only the fretting scar on the left contact surface is shown in Figure 5. For the 6.5 kN case, the contact surface includes the stick and slip zone, as illustrated in Figure 5c. The center of the contact surface remains sticky. Additionally, the severe wear marks only exist at the edge of the stick zone, which is obviously in partial slip condition. In addition, it can be seen that the severe wear marks exist on the entire contact surface under the cyclic load amplitude of 8.5 and 7.3 kN, which is known as the gross slip condition. These fretting scars indicate that the reduced load amplitude is an effective measure to improve the fretting fatigue properties. Similar results were found by Cortez and Massingham [43,44].

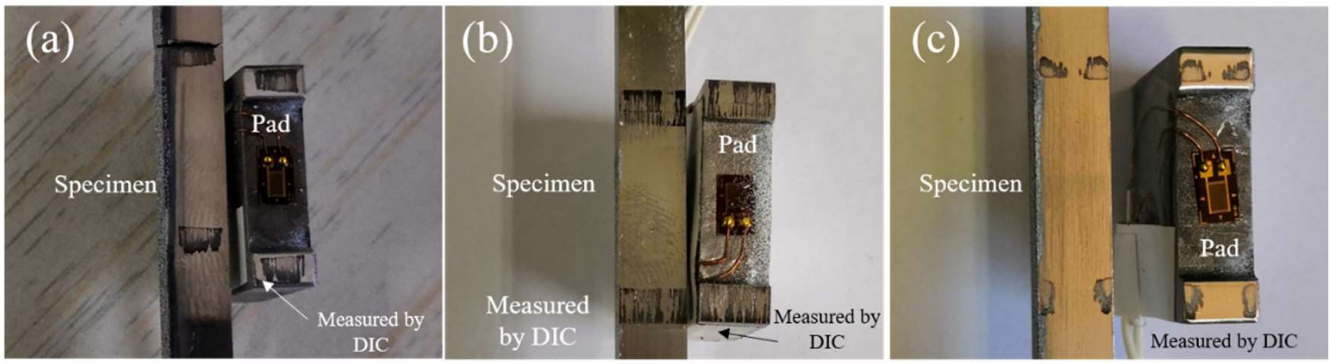


**Figure 5.** Fretting scar on the specimen and fretting pad for (**a**) *F*a = 8.5 kN, (**b**) *F*a = 7.3 kN, and (**c**) *F*a = 6.5 kN.

### 3.2. Tangential Force Coefficient

The tangential force coefficient (TFC) is a significant parameter as it affects the fretting response [45]. It was calculated using Equation (1):

$$\text{TFC} = \frac{Ft}{Fn} \quad (1)$$

where $Ft$ is the tangential force amplitude and $Fn$ is the normal contact force. They were obtained according to the strain during the test.

Figure 6 shows the evolution of the TFC during the test. In all load amplitude cases, the TFC at the initial stage was low, and their values were 0.1–0.2. This indicates that the slip occurs between the contact surfaces, which is caused by the high surface quality at the original state. Then, the TFC increases rapidly as the number of cycles increases. This large range of variation reveals that the wear appeared on the surface and the roughness deteriorated due to the slip on the contact surfaces at the beginning of the test. When the number of cycles reached about 1000, the TFC was gradually stabilized. This result reflects that the contact condition has become a stable state. On the other hand, the effect of cyclic load amplitude on the TFC response was also discussed in this paper. When the $Fa$ reduced from 8.5 to 7.3 kN, the steady-state value of the TFC did not change, and their values were both between 0.71 and 0.72. However, as the load amplitude reduced to 6.5 kN, the steady-state value of the TFC was 0.5. Hence, for the 6.5 kN case, the contact surfaces were in a partial slip state. In turn, the gross slip condition appeared at the 8.5 kN case. It is worth noting that, based on the TFC alone, the state of the slip plane cannot be determined. However, according to the fretting scar, the gross slip occurred at the 6.5 kN test.

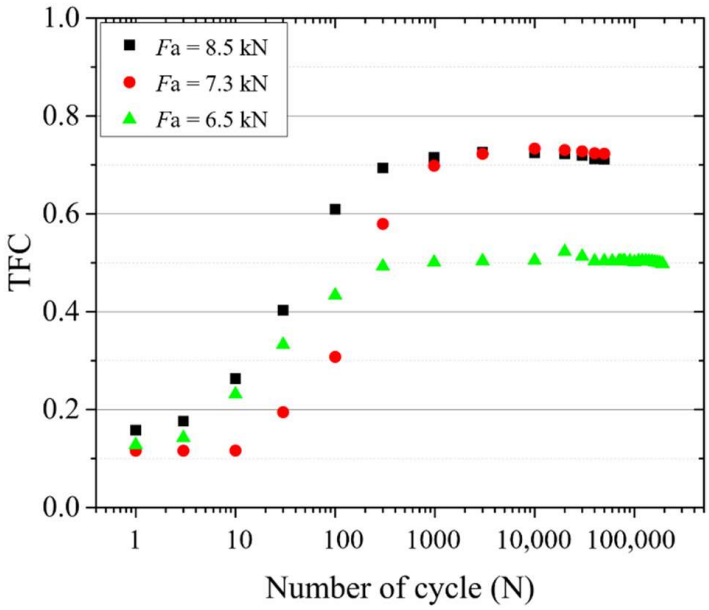


**Figure 6.** Evolution of TFC with the cycle number during the test.

### 3.3. Displacement Field

The vertical displacement (v) field of the observation area obtained by DIC postprocessing is depicted in Figure 7a. The cyclic load value was 7.3 kN. As shown in the figure, the dog-bone specimen was located on the right side of the area, and the fretting pad appeared on the left side. Thus, the contact surface was observed in this area. As expected, a bandlike form displacement field appeared in the observation area of the specimen. Since the cyclic load was applied to the specimen through the movement of the lower chuck, the vertical displacement near the lower side was higher. There is a nondata area near contact surfaces due to the divided calculation area and the limitation of a postprocessing

algorithm. Besides, the vertical displacement of the fretting pad is lower than that of the specimens.

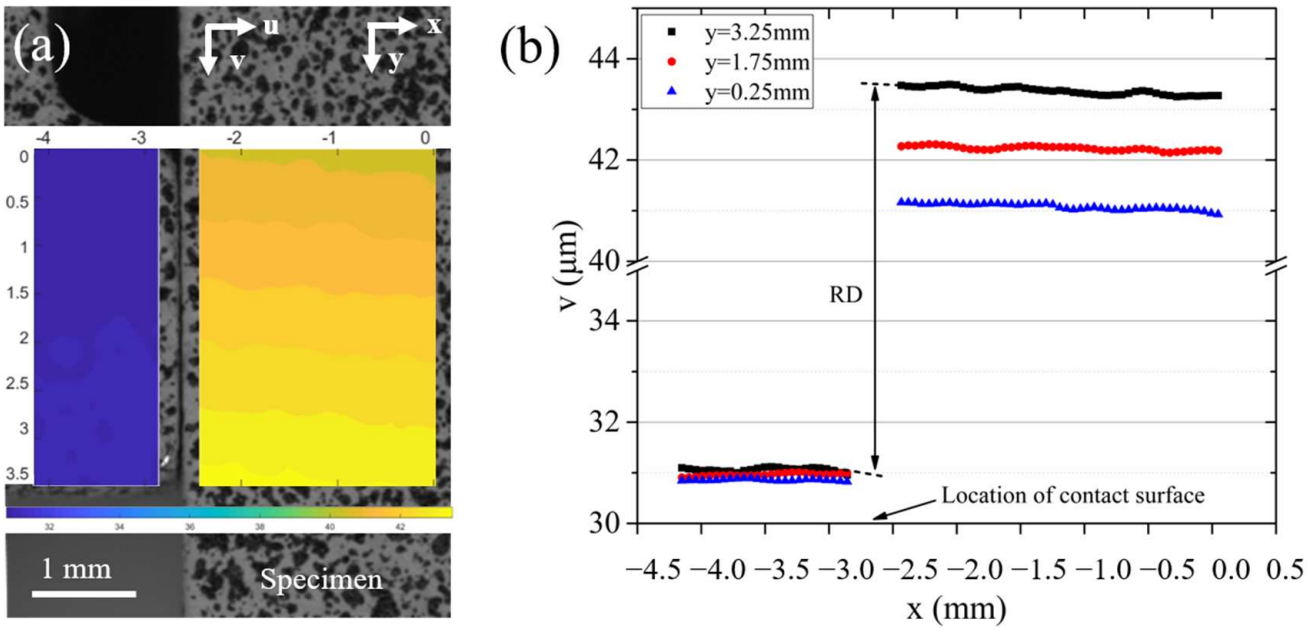


**Figure 7.** (**a**) Vertical displacement cloud of the observation area and (**b**) distribution of vertical displacement along the x-direction for the 7.3 kN case (cycle 1).

In order to describe the relative displacement between the contact surfaces, the distribution of vertical displacement along the x-direction is shown in Figure 7b. It can be seen that the displacement variation of the fretting pad along the x-direction was lower than the specimen. Additionally, the vertical displacement increases with the y-coordinate increases, which is consistent with the cyclic load applied by the movement of the lower chuck. Besides, there is a value jump due to the contact surface. Despite the lack of data near contact surfaces, the displacement still exhibits a linear law, as shown in Figure 7b. Therefore, the vertical displacement of the specimen and fretting pad on the contact surfaces can be determined by linear fitting. Furthermore, the relative displacement (RD) between the contact surfaces can be obtained in this study as follows:

$$\mathrm{RD} = v_{\mathrm{specimen}} - v_{\mathrm{pad}} \tag{2}$$

where $v_{\mathrm{specimen}}$ and $v_{\mathrm{pad}}$ are the vertical displacement of the specimen and fretting pad on the contact surfaces, respectively.

At the same time, the displacement field was obtained along the thickness direction, but the displacement change was smaller than that of the contact surface. Consider that this work focuses on the fretting state of the contact surface. Therefore, the distribution in the thickness direction was not discussed in detail.

### *3.4. Hysteresis Loops*

Figure 8 shows the hysteresis loops of relative displacement and tangential force during the experiment for the 8.5 kN case. The tangential force was measured by the strain, and the relative displacement was determined based on the DIC measurement results mentioned above. As shown in Figure 8c, the tangential stiffness was defined as the slope of the hysteresis loop at the stick stage, which is as follows:

$$\mathrm{k} = \Delta F\mathrm{t}/\Delta\mathrm{RD} \tag{3}$$

where $\Delta F$t and ΔRD are the increments of tangential force and relative displacement.

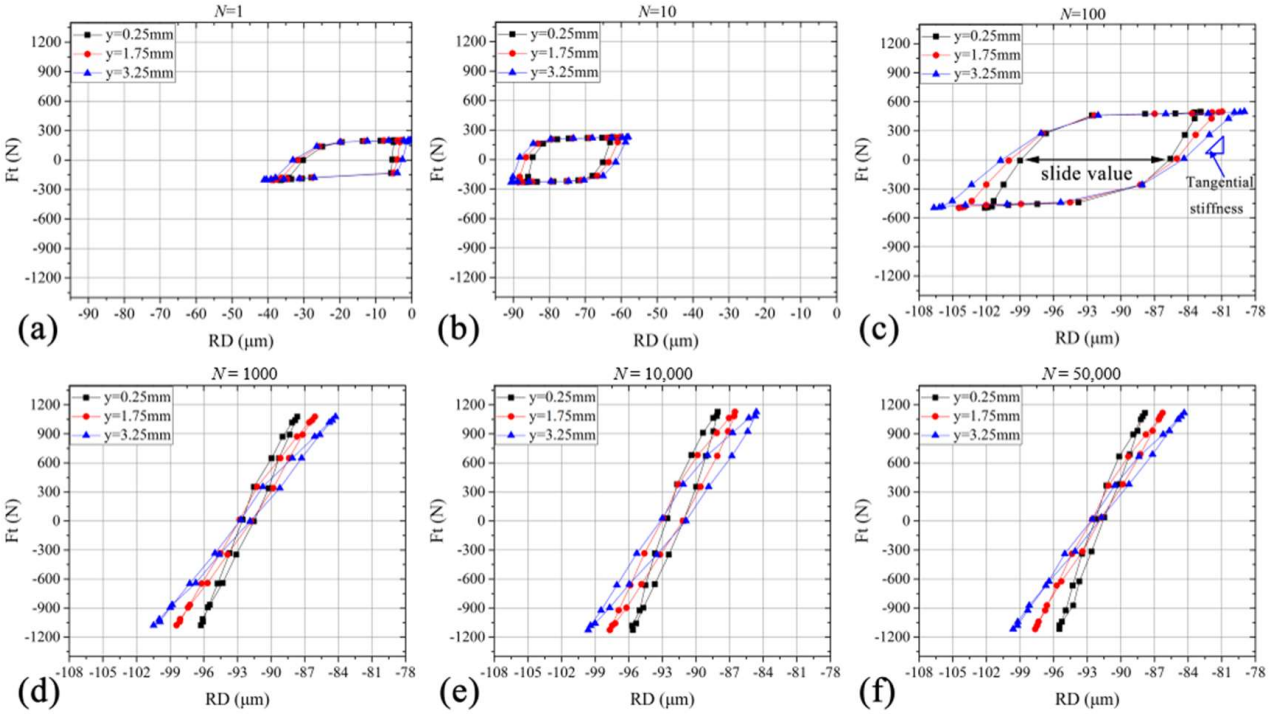


**Figure 8.** Hysteresis loops of tangential force (*F*t) in a function of relative displacement (RD) for the 8.5 kN case: (**a**) *N* = 1, (**b**) *N* = 10, (**c**) *N* = 100, (**d**) *N* = 1000, (**e**) *N* = 10,000, and (**f**) *N* = 50,000.

For cycle 1, the contact surface was in gross slip condition due to the parallelogram-like hysteresis loops at different positions. When the tangential frictional force was reduced to zero, the relative displacement cannot be fully recovered. With the increasing number of cycles, the tangential force gradually increased and stabilized at 1175 N after 10,000 cycles. Additionally, note that the hysteresis loops change from parallelogram to elliptical. In addition, the relative displacement between the contact surfaces increases when the y-coordinate increases. This reveals that the movement closer to the lower chuck was greater. Especially, the curve-enclosed area of the hysteresis loop represents the frictional energy loss during the experiment. It is worth noting that severe wear occurred during the early stage of the experiment. Subsequently, the energy loss decreases and stabilizes as the number of cycles increases.

The effect of cyclic load amplitude on the hysteresis loop was also explored in this paper. Figures 9 and 10 show the hysteresis loops for the 7.3 and 6.5 kN cases. For all three cases, the hysteresis loops exhibit the transformation from a parallelogram to an ellipse with the increasing load cycle. Additionally, these loops have a similar evolution process at different heights, as shown in Figures 9 and 10. However, for the 6.5 kN case, the shape of hysteresis loops became a straight line after 10,000 cycles. Further, the tangential force amplitude was stabilized at 950 N, which was lower than the 1175 N for other load conditions. These results reflect that the local contact surface was in stick condition. In addition, since the fretting pad cannot be completely symmetrical, self-equilibrium will occur on the contact surface, which leads to complicated changes in the relative displacement in the early stage. As such, the mean value of the RD was positive during the first 10 cycles and then became negative for the 7.3 kN case, as shown in Figure 9a,b. However, in all cases, the mean values were all negative at the stable stage. This is consistent with previous works [29,34].

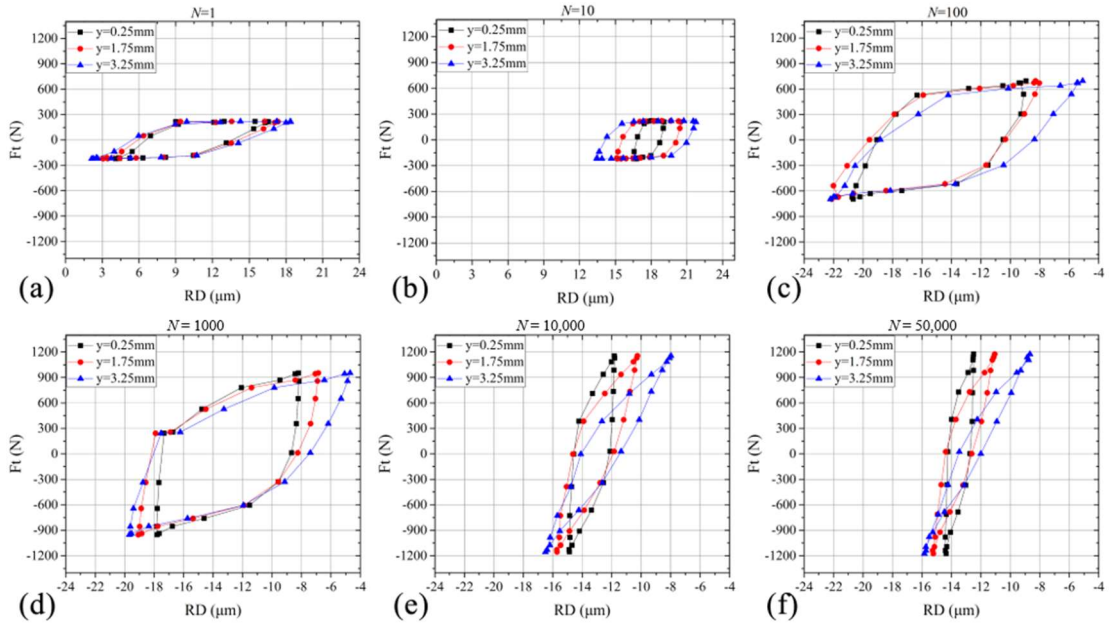


**Figure 9.** Hysteresis loops of tangential force (*F*t) in a function of relative displacement (RD) for the 7.3 kN case: (**a**) *N* = 1, (**b**) *N* = 10, (**c**) *N* = 100, (**d**) *N* = 1000, (**e**) *N* = 10,000, and (**f**) *N* = 50,000.

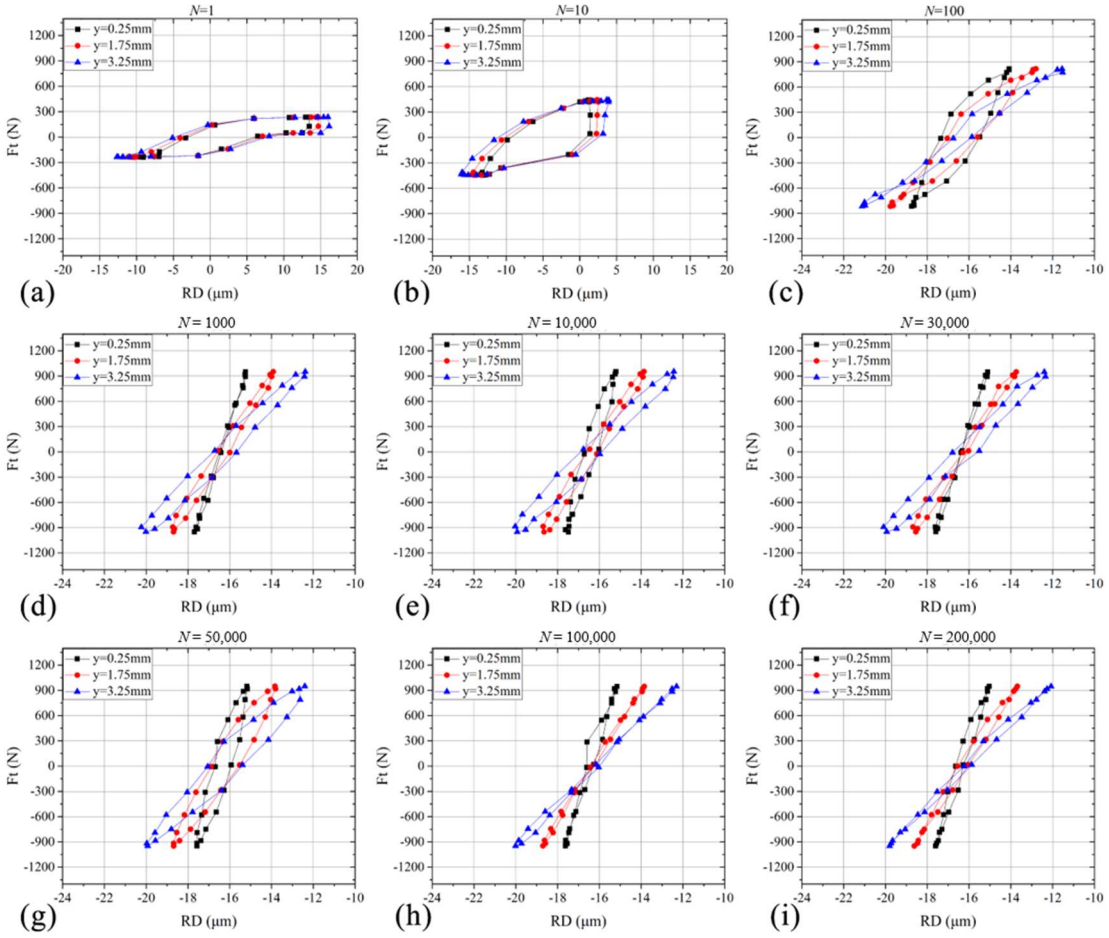


**Figure 10.** Hysteresis loops of tangential force (*F*t) in a function of relative displacement (RD) for the 6.5 kN case: (**a**) *N* = 1, (**b**) *N* = 10, (**c**) *N* = 100, (**d**) *N* = 1000, (**e**) *N* = 10,000, (**f**) *N* = 30,000, (**g**) *N* = 50,000, (**h**) *N* = 100,000, and (**i**) *N* = 200,000.

## 4. Discussion and Analysis

### *4.1. Definition of Slip Value and Tangential Stiffness*

Many studies have confirmed that slip amplitude and tangential contact stiffness are important parameters of contact properties. For example, Madge et al. investigated the effect of slip amplitude on fretting fatigue life [46,47]. Allara et al. used contact stiffness to evaluate the fretting fatigue response of turbine blades [48]. Meanwhile, lip value and tangential stiffness can be determined through the hysteresis loop, and their definitions can be found in Figure 8c. In this paper, these parameters were calculated by the hysteresis loops under different test conditions mentioned above.

### *4.2. Evolution of Relative Slip with the Cycle Number*

Relative slip is an important factor that characterizes the properties of fretting contact surfaces, and it is helpful to determine whether the contact point is stick or slip state. To illustrate the evolution law of relative slip, its change with the cycle number during the experiment at different cyclic load amplitudes is shown in Figure 11. It can be seen that there is a large relative slip at the beginning of the experiments. Then, for the 8.5 kN case, these values decrease sharply and stabilize as the number of cycles increases. This phenomenon indicates that the larger slide occurred in the initial stage. Additionally, with the further cycles, the slide between the contact surfaces decreases rapidly. This is because the debris adheres to the interface surfaces, which deteriorates the surface quality. When the state of the contact surface is stable, the variation of relative slip with the number of cycles becomes smaller. This is consistent with the evolution law of the TFC described above (see Figure 6). In addition, three curves of relative slip at different height positions (y-direction) are also shown in Figure 11a. Although the relative slip at y = 0.25 mm was lower than others, the evolution law of relative slip was still similar for the three curves. A more detailed discussion about the distribution of relative slip along the contact surfaces can be found later in Section 4.3.

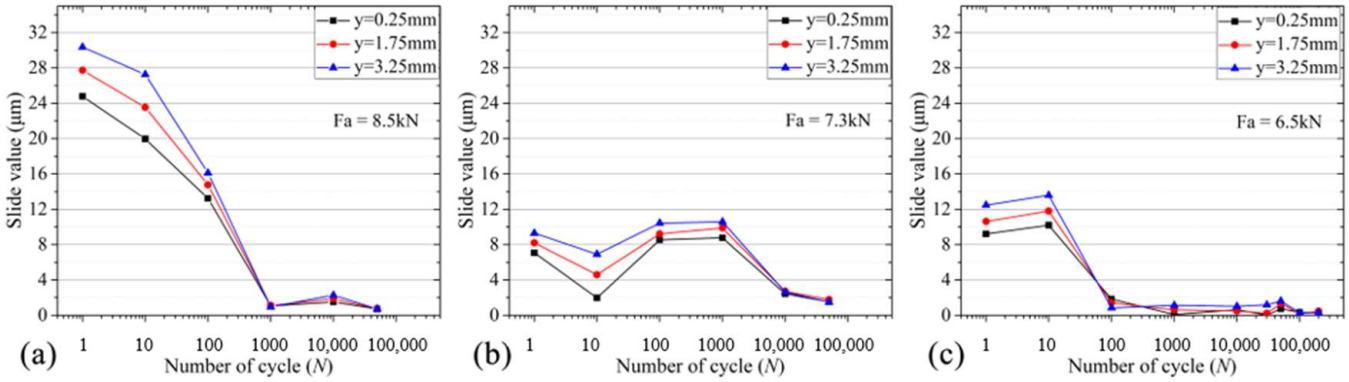


**Figure 11.** The evolution of relative slip with the cycle number during the test for the (**a**) 8.5 kN, (**b**) 7.3 kN, and (**c**) 6.5 kN cases.

In order to investigate the effect of the load amplitude on the fretting fatigue behavior, the relative slips at the 7.3 and 6.5 kN cases were also compared in Figure 11b,c. Obviously, there is a similar evolution law of relative slip as the cyclic load amplitude decreases. In all tests, the relative slip started from a relatively high value, but decreased rapidly and stabilized. However, this figure also reflects the difference in relative slip between the three tests. For instance, the relative slip at the beginning of the experiments for the 8.5 kN case was between 24 and 30 μm, values that were highest in both cases. When the load amplitude decreased, the relative slip at 1 cycle was reduced from about 28 to 10 μm. The highest relative slip at the initial stage indicates that there is more severe wear between the contact surfaces at 8.5 kN. This result is consistent with the fretting scar (see Figure 5) on the contact surfaces. It should be noted that the relative slip was no longer decreased when the load amplitude was reduced to 6.5 kN, and their values remained at about 10 μm

in cycle 1. However, the relative slip was stable after 100 cycles for the 6.5 kN case, instead of 10,000 cycles in the 7.3 kN case. Hence, a longer period of slide occurred on the contact surfaces, since the cyclic load amplitude increased from 6.5 to 7.3 kN. At the same time, it is worth noting that the relative slip increased slightly at the beginning of the experiment, as shown in Figure 8b. It is possible that self-equilibration occurred early in the experiment because of the incomplete symmetry of the fretting pad. Nonetheless, the overall trend is clear.

### *4.3. Distribution of Relative Slip along the Contact Surface*

Figure 12a shows the distribution of relative slip along the y-direction throughout all tests at 8.5 kN in order to further recognize the slip or stick state of the contact position. It can be seen from the figure that all relative slips increase as the y-coordinate increases. Before 100 cycles, the relative slip of the contact surfaces all exceeded 5 μm. This indicates that all points on the contact surfaces were in a slip state, which is known as gross slip condition. It provides an explanation for the dramatic increase in TFC at the beginning of the experiment. Then, the relative slip decreased rapidly as the experiment ran. Since the higher relative slip was near the lower chuck ($y$ = 3.25 mm), the upper side of the contact surface ($y$ = 0.25 mm) became stuck earlier. In contrast, other positions on the contact surfaces were still in a slip state. Therefore, the contact condition changes from a gross slip to a typical partial slip at this moment. Furthermore, when the number of cycles was higher than 10,000, the relative slip of all points on the interface surfaces was less than 2 μm, as shown in Figure 12a. This result shows that the entire surface was in a sticky condition after 10,000 cycles.

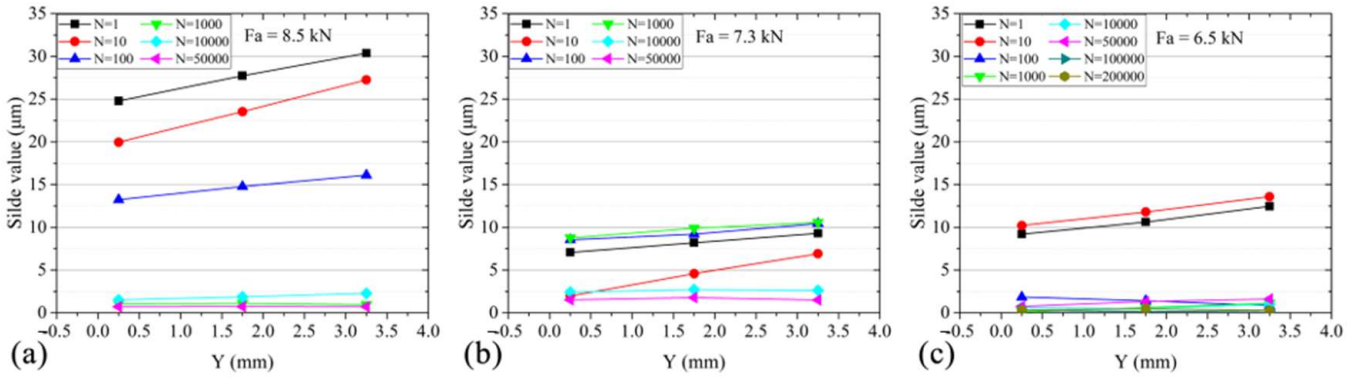


**Figure 12.** Distribution of relative slip along the contact surface for the (**a**) 8.5 kN, (**b**) 7.3 kN, and (**c**) 6.5 kN cases.

The effect of load amplitude on the slide or stick state is also clearly shown in Figure 12. Despite that the relative slip at the same number of cycles was reduced, the upward trend along the contact surfaces was also observed at 7.3 and 6.5 kN. Besides, the fretting contact condition changes from the initial gross slip to a partial slip when the number of cycles increases. For example, when the load amplitude was reduced to 6.5 kN, the relative slip at different locations was below 5 μm after 100 cycles. This indicates that the contact surface was in gross slip for a shorter time at 6.5 kN, compared with the 7.3 kN case. Besides, it should be noted that all points on the surfaces became sticky when the relative slip was stabilized below 2 μm.

### *4.4. Tangential Contact Stiffness*

In order to further explore the contact properties under the fretting fatigue condition, the tangential contact stiffness obtained from the hysteresis loops is shown in Figure 13. Clearly, the tangential stiffness increased with the number of cycles at $F$a = 6.5 kN during the experiment, as shown in Figure 13a. One of the possible reasons for this effect was the increase in contact area throughout the test. Figure 13b shows the variation in tangential

stiffness versus the y-coordinate for the 6.5 kN case. It can be seen from the figure that there was a higher tangential stiffness at $y$ = 0.25 mm (near the lower chuck). This nonuniform distribution of stiffness can reflect the variation of contact pressure along the interface surface. In detail, the contact pressure decreases as the y-coordinate increases. This is consistent with the increase in relative slip along the contact surfaces for all tests. These results about tangential contact stiffness were also investigated by Kartal et al. [29].

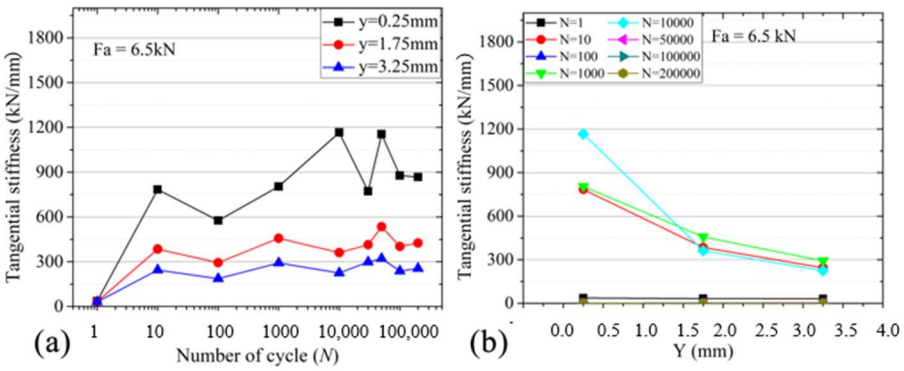


**Figure 13.** (**a**) Evolution of tangential stiffness with the number of cycles and (**b**) distribution of tangential stiffness along the contact surface for the 6.5 kN case.

## 5. Conclusions

In this study, an experimental method for accurately measuring the relative displacement between contact surfaces under the fretting fatigue condition was developed. The displacement field between the contact surfaces was measured by the DIC method. Through the distribution of displacement along the x-direction, it can be found that there was a value jump in the vertical displacement on the contact surface. Thus, the relative displacement between the specimen and fretting pad was determined by the linear fitting. The hysteresis loops of relative displacement and tangential force started from a parallelogram, then turned into an ellipse and stabilized into a straight line throughout all tests. Consequently, the DIC method was a feasible approach to acquire the distribution and evolution of relative slip in the fretting fatigue condition.

At the beginning of the test, the higher relative slip indicates that severe wear occurs on the contact surfaces, which is obtained from the hysteresis loops. Additionally, it was found that the value decreases markedly and stabilizes as the number of cycles increases. At the same time, the fretting condition of the contact surface exhibits a transition from gross slip to partial slip. Besides, the decreases in surface quality caused by wear lead to an increase in TFC. Hence, the evolution rule of the relative slip is in good agreement with the TFC. In order to investigate the effect of cyclic load amplitude on fretting fatigue properties, tests were carried out for three load amplitudes. Results show that the relative slip at the initial stage dropped sharply when the load amplitude was reduced from 8.5 to 7.3 kN. Compared with the 7.3 kN case, the partial slip condition appears earlier on the contact surface at $F$a = 6.5 kN, even if they have a similar relative slip at the initial stage. Therefore, the reduction of cyclic load amplitude plays an important role in the mitigation of fretting fatigue damage, which can affect the stick or slip state of the contact surfaces. The tangential contact stiffness obtained from hysteresis loops indicates the variation of contact pressure along the interface surface, which is consistent with the distribution of relative slip along the contact surface for all tests.

**Author Contributions:** Study concept and design: Y.S., Q.-N.H. and H.L. Acquisition of data: Y.S. Analysis and interpretation of data: Y.S. and S.-S.R. Drafting of the manuscript: Y.S. and S.-S.R. Critical revision of the manuscript for important intellectual content: L.-S.N. and H.-J.S. Statistical analysis: Z.-H.S. Obtained funding: H.-J.S. and H.I. Study supervision: H.-J.S., H.L., and H.I. All authors have read and agreed to the published version of the manuscript.

**Funding:** This work is financially supported by Mitsubishi Heavy Industries, Ltd., Japan, and the National Natural Science Foundation of China (Grant Nos. 12172193, 11632010, 11672151, 91860101), and National Science and Technology Major Project (Grant No. J2019-VI-0002-0115, 2017-VI-0003-0073).

**Institutional Review Board Statement:** Not applicable.

**Informed Consent Statement:** Not applicable.

**Data Availability Statement:** Not applicable.

**Conflicts of Interest:** The authors declare that they have no known competing financial interests or personal relationships that could have appeared to influence the work reported in this paper. The authors declare no conflict of interest.

## References

1. Waterhouse, R.B. *Fretting Fatigue*; Elsevier Science & Technology: Amsterdam, The Netherlands, 1981.
2. Nowell, D. *An Analysis of Fretting Fatigue*; University of Oxford: Oxford, UK, 1988.
3. Hills, D.A. Mechanics of fretting fatigue. *Wear* **1994**, *175*, 107–113. [CrossRef]
4. Foletti, S.; Beretta, S.; Gurer, G. Defect acceptability under full-scale fretting fatigue tests for railway axles. *Int. J. Fatigue* **2016**, *86*, 34–43. [CrossRef]
5. Ekberg, A. Fretting fatigue of railway axles—A Review of predictive methods and an outline of a finite element model. *Proc. Inst. Mech. Eng. Part F J. Rail Rapid Transit* **2004**, *218*, 299–316. [CrossRef]
6. Moraes, J.; Rao, H.M.; Jordon, J.; Barkey, M. High cycle fatigue mechanisms of aluminum self-piercing riveted joints. *Fatigue Fract. Eng. Mater. Struct.* **2017**, *41*, 57–70. [CrossRef]
7. Huang, L.; Bonnen, J.; Lasecki, J.; Guo, H.; Su, X. Fatigue and fretting of mixed metal self-piercing riveted joint. *Int. J. Fatigue* **2016**, *83*, 230–239. [CrossRef]
8. Oskouei, R.; Ibrahim, R. Improving fretting fatigue behaviour of Al 7075-T6 bolted plates using electroless Ni–P coatings. *Int. J. Fatigue* **2012**, *44*, 157–167. [CrossRef]
9. Peterka, P.; Krešák, J.; Kropuch, S.; Fedorko, G.; Molnar, V.; Vojtko, M. Failure analysis of hoisting steel wire rope. *Eng. Fail. Anal.* **2014**, *45*, 96–105. [CrossRef]
10. Rajasekaran, R.; Nowell, D. Fretting fatigue in dovetail blade roots: Experiment and analysis. *Tribol. Int.* **2006**, *39*, 1277–1285. [CrossRef]
11. Barella, S.; Boniardi, M.; Cincera, S.; Pellin, P.; Degive, X.; Gijbels, S. Failure analysis of a third stage gas turbine blade. *Eng. Fail. Anal.* **2011**, *18*, 386–393. [CrossRef]
12. Su, Y.; Han, Q.N.; Qiu, W.; He, Z.; Shang, Y.B.; Shi, H.J.; Niu, L.S. High temperature in-situ SEM observation and crystal plasticity simulation on fretting fatigue of Ni-based single crystal superalloys. *Int. J. Plast.* **2019**, *127*, 102645. [CrossRef]
13. Han, Q.; Rui, S.; Qiu, W.; Su, Y.; Ma, X.; He, Z.; Cui, H.; Zhang, H.; Shi, H. Subsurface crack formation and propagation of fretting fatigue in Ni-based single-crystal superalloys. *Fatigue Fract. Eng. Mater. Struct.* **2019**, *42*, 2520–2532. [CrossRef]
14. Zhou, Z.; Vincent, L. Mixed fretting regime. *Wear* **1995**, *181–183*, 531–536. [CrossRef]
15. Pasanen, A.; Lehtovaara, A.; Rabb, R.; Riihimäki, P. Friction behavior of quenched and tempered steel in partial and gross slip conditions in fretting point contact. *Wear* **2009**, *267*, 2200–2207. [CrossRef]
16. Sabelkin, V.; Mall, S. Investigation into relative slip during fretting fatigue under partial slip contact condition. *Fatigue Fract. Eng. Mater. Struct.* **2005**, *28*, 809–824. [CrossRef]
17. Fouvry, S.; Kapsa, P.; Vincent, L. Quantification of fretting damage. *Wear* **1996**, *200*, 186–205. [CrossRef]
18. Zhou, Z.; Nakazawa, K.; Zhu, M.; Maruyama, N.; Kapsa, P.; Vincent, L. Progress in fretting maps. *Tribol. Int.* **2006**, *39*, 1068–1073. [CrossRef]
19. Han, Q.N.; Rui, S.S.; Qiu, W.; Ma, X.; Su, Y.; Cui, H.; Zhang, H.; Shi, H. Crystal orientation effect on fretting fatigue induced geometrically necessary dislocation distribution in Ni-based single-crystal superalloys. *Acta Mater.* **2019**, *179*, 129–141. [CrossRef]
20. Vingsbo, O.; Söderberg, S. On fretting maps. *Wear* **1988**, *126*, 131–147. [CrossRef]
21. Jin, O.; Mall, S. Effects of slip on fretting behavior: Experiments and analyses. *Wear* **2004**, *256*, 671–684. [CrossRef]
22. Rengaraj, B.; Baba, S.; Okazaki, M. Influence of Crystal Orientation on Cyclic Sliding Friction and Fretting Fatigue Behavior of Single Crystal Ni-Base Superalloys. In *Superalloys 2016: Proceedings of the 13th Intenational Symposium of Superalloys*; John Wiley & Sons, Inc.: Hoboken, NJ, USA, 2016.
23. Su, Y.; Han, Q.N.; Zhang, C.C.; Shi, H.; Niu, L.S.; Deng, G.J.; Rui, S.S. Effects of secondary orientation and temperature on the fretting fatigue behaviors of Ni-based single crystal superalloys. *Tribol. Int.* **2018**, *130*, 9–18. [CrossRef]
24. Cai, Z.B.; Zhu, M.H.; Yang, S.; Xiao, X.B.; Lin, X.Z.; Yu, H.Y. In situ observations of the real-time wear of PMMA flat against steel ball under torsional fretting. *Wear* **2011**, *271*, 2242–2251. [CrossRef]
25. Han, Q.N.; Qiu, W.; He, Z.; Su, Y.; Ma, X.; Shi, H.J. The effect of crystal orientation on fretting fatigue crack formation in Ni-based single-crystal superalloys: In-situ SEM observation and crystal plasticity finite element simulation. *Tribol. Int.* **2018**, *125*, 209–219. [CrossRef]

26. Wittkowsky, B.U.; Birch, P.R.; Dominguez, J.; Suresh, S. An apparatus for quantitative fretting fatigue testing. *Fatigue Fract. Eng. Mater. Struct.* **1999**, *22*, 307–320. [CrossRef]
27. Popov, V.L. *Contact Mechanics and Friction*; Springer: Berlin/Heidelberg, Germany, 2010.
28. Kartal, M.E.; Mulvihill, D.M.; Nowell, D.; Hills, D.A. Determination of the Frictional Properties of Titanium and Nickel Alloys Using the Digital Image Correlation Method. *Exp. Mech.* **2010**, *51*, 359–371. [CrossRef]
29. Kartal, M.; Mulvihill, D.; Nowell, D.; Hills, D. Measurements of pressure and area dependent tangential contact stiffness between rough surfaces using digital image correlation. *Tribol. Int.* **2011**, *44*, 1188–1198. [CrossRef]
30. De Pauw, J.; De Waele, W.; Hojjati-Talemi, R.; De Baets, P. On the use of digital image correlation for slip measurement during coupon scale fretting fatigue experiments. *Int. J. Solids Struct.* **2014**, *51*, 3058–3066. [CrossRef]
31. Ding, J.; Bandak, G.; Leen, S.; Williams, E.; Shipway, P. Experimental characterisation and numerical simulation of contact evolution effect on fretting crack nucleation for Ti–6Al–4V. *Tribol. Int.* **2009**, *42*, 1651–1662. [CrossRef]
32. Pan, B.; Qian, K.; Xie, H.; Asundi, A. Two-dimensional digital image correlation for in-plane displacement and strain measurement: A review. *Meas. Sci. Technol.* **2009**, *20*, 062001. [CrossRef]
33. Blaber, J.; Adair, B.S.; Antoniou, A. Ncorr: Open-Source 2D Digital Image Correlation Matlab Software. *Exp. Mech.* **2015**, *55*, 1105–1122. [CrossRef]
34. Juoksukangas, J.; Lehtovaara, A.; Mäntylä, A. Applying the digital image correlation method to fretting contact for slip measurement. *Proc. Inst. Mech. Eng. Part J J. Eng. Tribol.* **2016**, *231*, 509–519. [CrossRef]
35. Juoksukangas, J.; Lehtovaara, A.; Mäntylä, A. A comparison of relative displacement fields between numerical predictions and experimental results in fretting contact. *Proc. Inst. Mech. Eng. Part J J. Eng. Tribol.* **2016**, *230*, 1273–1287. [CrossRef]
36. De Crevoisier, J.; Swiergiel, N.; Champaney, L.; Hild, F. Identification of in situ frictional properties of bolted assemblies with digital image correlation. *Exp. Mech.* **2012**, *52*, 561–572. [CrossRef]
37. Cuevas Arteaga, C.; Rodríguez, J.A.; Clemente, C.M.; Segura, J.A.; Urquiza, G.; Hamzaoui, Y.E. Estimation of useful life in turbines blades with cracks in corrosive environment. *Eng. Fail. Anal.* **2013**, *35*, 576–589. [CrossRef]
38. ASTM. *Standard Test Methods for Tension Testing of Metallic Materials*; ASTM International: West Conshohocken, PA, USA, 2016; Volume E8/E8M-162016.
39. JSME. *JSME Standard Method of Fretting Fatigue Testing*; Japan Society Mechanical Engineers: Tokyo, Janpan, 2002; Volume JSME S 015-20022002.
40. Nix, K.J.; Lindley, T.C. The Application of Fracture Mechanics to Fretting Fatigue. *Fatigue Fract. Eng. Mater. Struct.* **1985**, *8*, 143–160. [CrossRef]
41. Pan, B. Recent Progress in Digital Image Correlation. *Exp. Mech.* **2010**, *51*, 1223–1235. [CrossRef]
42. Chu, T.C.; Ranson, W.F.; Sutton, M.A. Applications of digital-image-correlation techniques to experimental mechanics. *Exp. Mech.* **1985**, *25*, 232–244. [CrossRef]
43. Massingham, M.; Irving, P. The effect of variable amplitude loading on stress distribution within a cylindrical contact subjected to fretting fatigue. *Tribol. Int.* **2006**, *39*, 1084–1091. [CrossRef]
44. Cortez, R. Investigation of variable amplitude loading on fretting fatigue behavior of Ti-6Al-4V. *Int. J. Fatigue* **1999**, *21*, 709–717. [CrossRef]
45. Mubarak Ali, M.; Ganesh Sundara Raman, S.; Pathak, S.D.; Gnanamoorthy, R. Influence of plasma nitriding on fretting wear behaviour of Ti–6Al–4V. *Tribol. Int.* **2010**, *43*, 152–160. [CrossRef]
46. Madge, J.; Leen, S.; McColl, I.; Shipway, P. Contact-evolution based prediction of fretting fatigue life: Effect of slip amplitude. *Wear* **2007**, *262*, 1159–1170. [CrossRef]
47. Madge, J.; Leen, S.; Shipway, P. The critical role of fretting wear in the analysis of fretting fatigue. *Wear* **2007**, *263*, 542–551. [CrossRef]
48. Allara, M. A model for the characterization of friction contacts in turbine blades. *J. Sound Vib.* **2008**, *320*, 527–544. [CrossRef]